Annual Review of Analytical Chemistry

Solving the Structure and Dynamics of Metal Nanoparticles by Combining X-Ray Absorption Fine Structure Spectroscopy and Atomistic Structure Simulations

J. Timoshenko,[1] Z. Duan,[2,3] G. Henkelman,[2,3] R.M. Crooks,[2] and A.I. Frenkel[1,4]

[1]Department of Materials Science and Chemical Engineering, Stony Brook University, Stony Brook, New York 11794, USA; email: anatoly.frenkel@stonybrook.edu

[2]Department of Chemistry and Texas Materials Institute, University of Texas at Austin, Austin, Texas 78712, USA

[3]Institute for Computational and Engineering Sciences, University of Texas at Austin, Austin, Texas 78712, USA

[4]Division of Chemistry, Brookhaven National Laboratory, Upton, New York 11973, USA

Annu. Rev. Anal. Chem. 2019. 12:501–22

First published as a Review in Advance on January 30, 2019

The *Annual Review of Analytical Chemistry* is online at anchem.annualreviews.org

https://doi.org/10.1146/annurev-anchem-061318-114929

Keywords

X-ray absorption spectroscopy, EXAFS, nanoparticles, structure, density functional theory, molecular dynamics, reverse Monte Carlo

Abstract

Extended X-ray absorption fine structure (EXAFS) spectroscopy is a premiere method for analysis of the structure and structural transformation of nanoparticles. Extraction of analytical information about the three-dimensional structure and dynamics of metal–metal bonds from EXAFS spectra requires special care due to their markedly non-bulk-like character. In recent decades, significant progress has been made in the first-principles modeling of structure and properties of nanoparticles. In this review, we summarize new approaches for EXAFS data analysis that incorporate particle structure modeling into the process of structural refinement.

1. INTRODUCTION

NP: nanoparticle

XAS: X-ray absorption spectroscopy

EXAFS: extended X-ray absorption fine structure

DFT: density functional theory

MD: molecular dynamics

MC: Monte Carlo

PDF: pair distribution function

Improved and increasingly accessible synchrotron radiation sources and high-resolution electron microscopy facilities provide new fundamental insights into nanoparticle (NP) structure and function that, in turn, have led to new ways of thinking about the technologies that employ these materials. The unique advantage of NPs is that their magnetic, electrical, optical, chemical, and catalytic properties can be tuned by changing NP shape, size, and composition. Indeed, the properties and potential applications of NPs depend strongly on their atomic structure, which can be very different from the corresponding bulk material. Understanding the atomic structure and dynamics of NPs is, therefore, important for understanding and controlling their function. Moreover, it is now well established that the structure of NPs can evolve over time, particularly in applications like catalysis, wherein reactive chemicals come into contact with the NP surface. Accordingly, analytical methods that can observe such chemical and structural changes under working (operando) conditions have become increasingly important (1–5). The choice of tools for investigating the local structure of small (1–3 nm) NPs is rather restricted, and the number of these tools that can be applied in situ is even more limited (6). X-ray absorption spectroscopy (XAS) (7–9) is one of the few analytical techniques that has been found to be useful in this regard. In particular, extended X-ray absorption fine structure (EXAFS) spectroscopy provides unique information on the distribution of atoms within the NP and the static and dynamic disorder that arises from structural perturbations caused by the environment. XAS is also a much less destructive probe compared to, e.g., electron microscopy. For these reasons, EXAFS spectroscopy has been widely applied to structural investigations of NPs and to correlate NP structure with chemical and catalytic properties (10–12).

As the sophistication of EXAFS analysis methods and the corresponding level of detailed information about NP architecture have expanded, the limitations of existing approaches become apparent. This is most obvious for NPs having sizes below several nanometers where non-bulk-like phenomena have been observed (13, 14). For example, many structural parameters are required to provide a complete description of the three-dimensional (3D) structure of NPs. Additionally, the heterogeneous environments of surface and core atoms and the resulting strain and structural relaxation result in complex, markedly asymmetric distributions of interatomic distances. Conventional data analysis approaches are unable to fully account for these factors and thus do not extract the maximum amount of information from EXAFS spectra (13, 15, 16).

At the same time, recent years have seen a rise in the importance and availability of atomic-level simulations of atomic and electronic structure and properties of NPs. In fact, theoretical modeling approaches are now used to fill the gaps in experimental data (6, 17). For example, the use of ab initio simulations within the density functional theory (DFT) formalism allows one to model relaxation processes in metallic NPs, and it has been used to predict the properties and structure of nanosized catalysts (18–20). Molecular dynamics (MD) and Monte Carlo (MC) simulations using interatomic forces that are derived either from ab initio calculations (15, 18) or from empirical force fields (17, 21–23) can be employed, in turn, to model thermal disorder and anharmonic effects. Thus, theoretical modeling can be a very powerful tool to advance our understanding of the local structure and dynamics in small NPs.

The structure models obtained in such simulations, however, must be validated by experimental data. Although a number of different techniques can be used for this purpose [e.g., total scattering experiments coupled to atomic pair distribution function (PDF) analysis (6)], the use of EXAFS may be advantageous due to its chemical sensitivity and high sensitivity toward the arrangement of nearest neighbors and many-atom distribution functions. Moreover, experimental EXAFS data can be directly incorporated into the structural refinement and modeling process using approaches

such as reverse Monte Carlo (RMC) (24–26). Combining RMC and MD (MC) approaches allows one to find the optimal structure models that agree with experimental data and that are physically reasonable (27).

To summarize, atomic-scale simulation of nanomaterial structure, guided by XAS data, is a new and rapidly developing field. The importance of and growing interest in such studies are supported by a number of recent publications devoted to this topic (15, 17, 19, 26, 28–45). The approaches described in these articles often rely on similar ideas, but their implementation varies because such combined studies are still a relatively new tool for modeling NP structure. The main goals of this review are to summarize the existing knowledge base and some success stories in this field and to stimulate further development of techniques that combine experimental studies with insights from theoretical modeling to provide a deeper understanding of NP structure and dynamics. Another important goal of this review is to show that conventional, easily implemented EXAFS analysis methods must be treated with caution when applied to complex, intrinsically heterogeneous nanomaterials.

RMC: reverse Monte Carlo

RDF: radial distribution function

2. EXTENDED X-RAY ABSORPTION FINE STRUCTURE DATA ANALYSIS

The attractiveness of EXAFS data analysis for quantitative structural studies of a broad range of materials relies, in part, on the fact that a simple and quite accurate relationship directly links the descriptors of material structure to EXAFS features. In a commonly used approach (7), experimentally measured, background-subtracted, and edge-step-normalized EXAFS spectrum χ is expressed as a sum of contributions of photoelectron scattering paths connecting the X-ray absorbing atom to its neighboring atoms:

$$\chi(k) = \sum_p \chi_p(k), \qquad 1.$$

where the photoelectron wavenumber is $k = \sqrt{\frac{2m}{\hbar^2}(E - E_0)}$, m is electron mass, $\hbar$ is Planck's constant, E is the energy of an absorbed X-ray photon, and $E - E_0$ is the energy of an excited photoelectron. This sum includes contributions from single-scattering paths, as well as contributions from multiple-scattering paths, wherein electrons interact with two or more neighboring atoms. For the single-scattering paths, the contribution of each path can then be expressed as (9)

$$\chi_p(k) = \frac{S_0^2}{k} \int_0^\infty f_p(k,R)\, g_p(R)\, e^{-\frac{2R}{\lambda_p(k)}} \sin\left[2kR + \phi_p(k,R)\right] \frac{dR}{R^2}. \qquad 2.$$

The integration in Equation 2 is carried out over the distance in the radial direction away from the X-ray absorber. The functions $f_p(k,R)$ and $\phi_p(k,R)$ characterize the changes in the amplitude and phase of the photoelectron upon scattering, while $\lambda_p(k)$ is an effective mean free path for the photoelectron that accounts for the reduction of EXAFS amplitude resulting from the finite lifetime of the excitation and all inelastic interactions of the photoelectron. The functions $f_p(k,R)$, $\phi_p(k,R)$, and $\lambda_p(k)$ can be calculated with good accuracy using ab initio codes such as FEFF (7, 46). The passive electron reduction factor S_0^2 in Equation 2 describes the reduction of EXAFS amplitude due to the perturbation of other electrons upon excitation of the core electron, and it can be obtained from the analysis of reference materials. Finally, $g_p(R)$ is the bond-length distribution, or the radial distribution function (RDF), which is a probability density of finding an atom of a

specific type at distance R from the absorbing atom. Its normalization is carried out via the integral

CN: coordination number

$$N_p = \int_{R_1}^{R_2} g_p(R)\,\mathrm{d}R. \qquad 3.$$

Equation 3 provides the number of nearest neighbors N_p within a specific coordination shell of radius $R_1 < R < R_2$. The finite width of the coordination shell characterizes the interatomic bond length disorder. Because the lifetime of the excited photoelectron (~1 fs) is several orders of magnitude shorter than the characteristic times of atomic vibrations (on the order of picoseconds), EXAFS does not distinguish between the bond length disorder caused by the thermal motion of atoms (thermal or dynamic disorder) versus the static disorder caused by the frozen deviations of the bond length from the average. Thus, $g_p(R)$ describes both the structure and dynamics of the material (7).

Equation 2 can be generalized to describe multiple-scattering contributions. In this case, however, one needs to consider that the functions f_p and ϕ_p will depend not only on the path length R, but also on the relative positions of scattering atoms (e.g., bonding angles). Thus, instead of the RDF, a many-atomic probability distribution function, $g_p(\mathbf{R})$ must be used in Equation 2.

Owing to Equations 1 and 2, it is relatively easy to calculate the theoretical EXAFS spectrum for each atomistic structure. Typically, however, EXAFS analysis is used to solve a much more difficult, inverse problem: Given the experimentally obtained EXAFS, how does one find a corresponding representative atomistic structure? Considering the nonlinear nature of Equation 2 and that many parameters are present in Equations 1 and 2, it is a challenging task, often prone to artifacts and numerical issues.

The conventional approach to EXAFS analysis is to parameterize all $g_p(R)$ functions and to fit the parameters of the distributions using a nonlinear least square procedure so that the theoretical spectrum, modeled according to Equations 1 and 2, matches the experimental data as well as possible (8–11, 47, 48). For moderately ordered materials the $g_p(R)$ function in Equation 2 can be approximated by a Gaussian function, and Equation 2 can be rewritten in its commonly used form (7):

$$\chi_p(k) = \frac{N_p S_0^2}{kR_p^2} f_p(k, R_p)\, e^{-\frac{2R_p}{\lambda_p(k)}} e^{-2\sigma_p^2 k^2} \sin\left[2kR_p + \phi_p(k, R_p)\right], \qquad 4.$$

where N_p is the average coordination number (CN) for the given coordination shell, R_p is an average interatomic distance, and σ_p^2 is the mean-square relative displacement factor, also known as the Debye-Waller factor, which accounts for the combined thermal and static disorder effects. The parameters N_p, R_p, and σ_p^2 are then used to characterize the local structure and bond dynamics of the material.

3. LIMITATIONS OF CONVENTIONAL EXTENDED X-RAY ABSORPTION FINE STRUCTURE DATA ANALYSIS FOR NANOPARTICLES

EXAFS fitting works well for materials with well-defined atomic arrangements in the nearest few coordination shells, such as crystalline materials. In nanostructured materials, however, much more complex, non-Gaussian shapes of bond-length distributions are common. These non-Gaussian distributions can be either static or dynamic in origin or both. For example, structure relaxation due to surface tension in metallic NPs usually results in shortening of interatomic

distances in the atomic layers that are close to the surface, but this effect is much smaller for atoms in the core (13, 49–51). Moreover, a strong anisotropy of atomic vibrations may originate from the asymmetric potential energy surfaces for atoms at the NP surface (52). An additional contribution to the asymmetry of the bond-length distribution arises from the interactions of NPs with the support, ligands, and/or adsorbates (18). The failure to account for these effects in EXAFS analysis may result in significant artifacts and incorrect conclusions.

AIMD: ab initio molecular dynamics

To assess the importance of this problem, one plausible strategy is to apply conventional EXAFS fitting procedures to theoretically constructed spectra, where the correct answer—the true RDF—is known in advance. Such model data can be generated through Equations 1 and 2, where the RDFs are obtained, e.g., by MD simulations (14, 15, 18, 26, 53–57). An example of such a model RDF for icosahedral Au_{147} NPs is shown in **Figure 1*a*** (see Section 5 for more details on MD). The asymmetry of the RDF peaks is clearly visible. After the RDF is integrated and a model EXAFS spectrum is obtained, one can apply conventional EXAFS fitting and compare the values of the best-fit parameters with those corresponding to the original bond-length distribution. Using this approach in the 1990s, Clausen, Nørskov, and colleagues (14, 52–55) pointed out that, in metallic NPs, neglecting the non-Gaussian effects results in underestimation of interatomic distances, CNs, and disorder factors. A similar approach was recently used in the study of Au_{147} nanoparticles by Timoshenko & Frenkel (26) (**Figure 1*b***). The effects of asymmetric static disorder were analyzed in a study by Yevick & Frenkel (13), where the fitting of model data, constructed by systematically distorting a model gold cluster structure, was carried out. Similar results were also recently obtained for the model data constructed in ab initio MD (AIMD) simulations for thiolated gold clusters (15, 18), with special attention paid to the contribution to the total disorder from interactions between gold atoms and ligands. One existing approach to correct for these effects relies on modeling $g_p(R)$ with more complex functions rather than a simple Gaussian, e.g., skewed Gaussian (58, 59) or even asymmetric gamma functions (21, 60–63). However, although these approaches may work in some specific cases [when a reasonable parameterization of $g_p(R)$ for

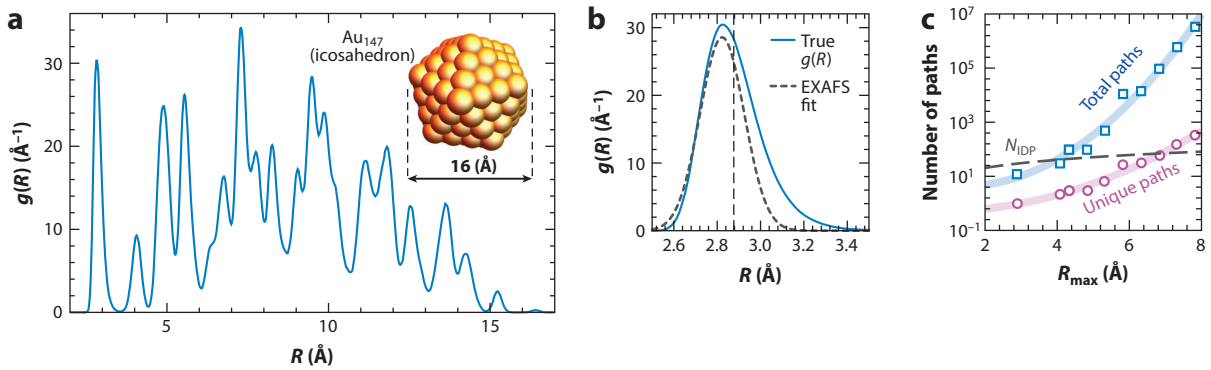

Figure 1

Limitations of EXAFS analysis. RDF $g(R)$ for Au atoms in icosahedral Au_{147} nanoparticle modeled in classical molecular dynamics simulations (26) is shown in panels *a* and *b*. Asymmetric shapes or RDF peaks cannot be reproduced by conventional EXAFS fitting in Gaussian approximation (*b*; *gray dotted line*), which underestimates coordination number (area under RDF peak) and yields shorter average Au–Au distance than the true value (*b*; *vertical dashed line*) (26). In panel *c*, the dependence of the number of scattering paths on R_{max} used for the analysis for bulk Au is compared with the maximal number of structure parameters N_{IDP} allowed by the Nyquist theorem (64). Because some of the paths in bulk structure are equivalent by symmetry, we show the total number of paths and number of unique (nonequivalent) paths separately. Abbreviations: EXAFS, extended X-ray absorption fine structure; RDF, radial distribution function.

the particular system is guessed by intuition or luck], they cannot be considered a general solution to the NP structure problem.

The second challenge is related to the number of scattering paths included in the analysis (Equation 1). If one limits the analysis by including contributions with R_p values up to R_{max} only, then the number of scattering paths grows exponentially with R_{max} (64) (**Figure 1*c***). The radius of the first coordination shell is significantly shorter than the radii of more distant coordination shells; thus, the first single-scattering contribution can usually be singled out by Fourier filtering and analyzed independently on the other paths. It is not the case, however, for the contributions of more distant coordination shells, because the single-scattering and multiple-scattering paths that correspond to those shells overlap strongly in the same R range. Their structural parameters should be refined concurrently (47, 60), which results in strong correlations in the fitting parameters and renders the entire analysis procedure unstable. According to the Nyquist theorem, the relevant number of independent data points in an EXAFS spectrum within a given spectral interval is defined by its k range, Δk, and R range, ΔR : $N_{IDP} = 2\Delta k \Delta R/\pi$ (64, 65). Hence, the number of fitting variables should not exceed the value of N_{IDP} or else the fitting results will be ill defined. Because N_{IDP} increases approximately linearly with increasing R_{max}, while the number of fitting parameters grows exponentially (unless multiple constraining relationships between the variables are applied), EXAFS analysis is limited to a range of just a few angstroms away from the absorbing atom. Another complication caused by the contribution of multiple-scattering effects is its above-mentioned sensitivity to bonding angles, which is especially important for materials with linear, or nearly linear, chains of atoms (66–68).

The final challenge is interpreting the fitting results obtained by conventional analysis. In the case of well-defined materials, such as homogeneous, single-phase bulk solids, these results provide corrections to the known average structure. In the case of nanomaterials, such average structures themselves are not known. In principle, to fully characterize the 3D structure of an NP consisting of N atoms, $3N$ atomic coordinates are required. This is, however, impossible to uniquely obtain from the handful of structural parameters yielded by an EXAFS fit without additional information and assumptions. A commonly used approach to link the CNs, obtained from EXAFS fitting, to a 3D structure is to approximate the NP shape with a regular polyhedron. For such a model the particle-averaged CNs can be easily calculated and contrasted with the results of EXAFS data analysis, providing information on particle size (10, 69–71), shape (10, 69), and alloying motifs in heterometallic particles (10, 34, 48). For realistic NPs, the presence of different types of atoms, vacancies, and disorder effects, along with NP interactions with the support and adsorbates, makes the regular, undistorted polyhedron a poor approximation of particle geometry. As discussed in the next sections, more advanced approaches, such as RMC and DFT simulations and MD and MC methods, are thus required to link the experimentally observed EXAFS features to 3D structural arrangements of atoms.

In addition to the foregoing factors, the assumption that the obtained EXAFS signal can be attributed to a single, well-defined particle model may result in overinterpretation of the data, because actual NPs coexist in multiple sizes, shapes [e.g., isomers in ultrasmall clusters (72)], and compositions (10). This sample-averaging problem is also important for more advanced modeling approaches discussed below. To deal with this issue, it is crucial to independently verify the homogeneity of the sample [e.g., by scanning transmission electron microscopy (STEM)] (10, 11, 73). Studies of well-defined model NP systems, prepared by dendrimer and inverse-micelle encapsulation techniques (74–77), peptide templating methods (30, 78), and DNA-assisted particle assembly (79), among others, enable precise calibration of such artifacts.

4. REVERSE MONTE CARLO SIMULATIONS

4.1. Reverse Monte Carlo Basics

RMC is a structure optimization technique for finding structure models in which theoretically calculated, structure-related properties are in good agreement with experimental data. RMC was introduced by McGreevy and Pusztai (80, 81) for the analysis of X-ray and neutron scattering data in disordered systems, but its potential for EXAFS analysis was realized almost immediately (24).

In RMC, an initial 3D structure model is proposed, and then it is iteratively modified by proposing random changes (e.g., atomic displacements or swapping of two atoms). After each such change, the cost function Δ_{new} is evaluated and compared with the corresponding cost function Δ_{old} that was evaluated for the structure model before the move was made. As a cost function, one can use, for example, the difference between partial CNs extracted from experimental EXAFS and those calculated for the model (82) or, more directly, the squared Euclidean distance $\Delta = \sum_i |\chi_i^{exp} - \chi_i|^2$ between experimental EXAFS χ_{exp} and theoretical spectrum χ calculated according to Equations 1 and 2 (24, 83). If EXAFS data from different absorption edges are available (e.g., for bimetallic particles), they can be used simultaneously by defining $\Delta = w_A\Delta_A + w_B\Delta_B$, where Δ_A and Δ_B are partial cost functions, calculated for metals A and B, respectively, while w_A and w_B are weights, which can be chosen to be different (e.g., if one spectrum has a significantly lower quality than the other).

By comparing Δ_{new} and Δ_{old}, a decision is made whether the proposed change should be accepted or the system should be returned to the previous state. For this purpose, the so-called Metropolis algorithm (84) is commonly used. Specifically, the move is accepted if $\Delta_{new} < \Delta_{old}$ (i.e., the new structure model fits experimental observations better) and also if $\Delta_{new} > \Delta_{old}$, but $\exp(-\frac{\Delta_{new}-\Delta_{old}}{T}) > \rho$, where ρ is a randomly generated number between 0 and 1, and T is a scaling factor. The acceptance of some of the moves that worsen the agreement between simulated and experimental results allows the system to escape some local minima and to better explore the configurational space (80). A scheme of the RMC process for EXAFS analysis is shown in **Figure 2*a***.

RMC-based analysis has several advantages with respect to conventional EXAFS fitting. First, no assumptions about the shapes of RDFs are required. Second, RMC immediately yields a 3D-structure model of the material, which can be used to extract commonly used parameters (R_p and σ_p^2). It can also be used for more advanced analysis such as determining the asymmetry and anisotropy of atomic displacements (25, 45, 85) and as a direct input for DFT-based calculation of the electronic and chemical properties of materials. Third, because the variables of the model are atomic coordinates, the number of unknowns does not depend on the number of scattering paths included in the analysis. Therefore, analysis of distant coordination shells can be accomplished as easily as the analysis of the first coordination shell contribution, and angular dependencies of multiple-scattering paths can also be treated explicitly (83). Finally, the RMC method allows one to easily implement many constraints to ensure that the resulting structure model is physically reasonable and does not contradict the results of other experimental techniques (e.g., X-ray diffraction) (83, 86). For example, one can force the interatomic distances and bond angles to be within the physically reasonable ranges (87) or preserve a specific number of nearest neighbors around each atom (81). Even more information can be introduced by using the so-called hybrid-RMC method (17, 27, 88) where, in addition to determination of the discrepancy between experimentally observed and theoretically calculated properties for each model, the corresponding energy is also calculated. In this case, energetically unfavorable configurations are penalized by additional contribution to the cost function Δ.

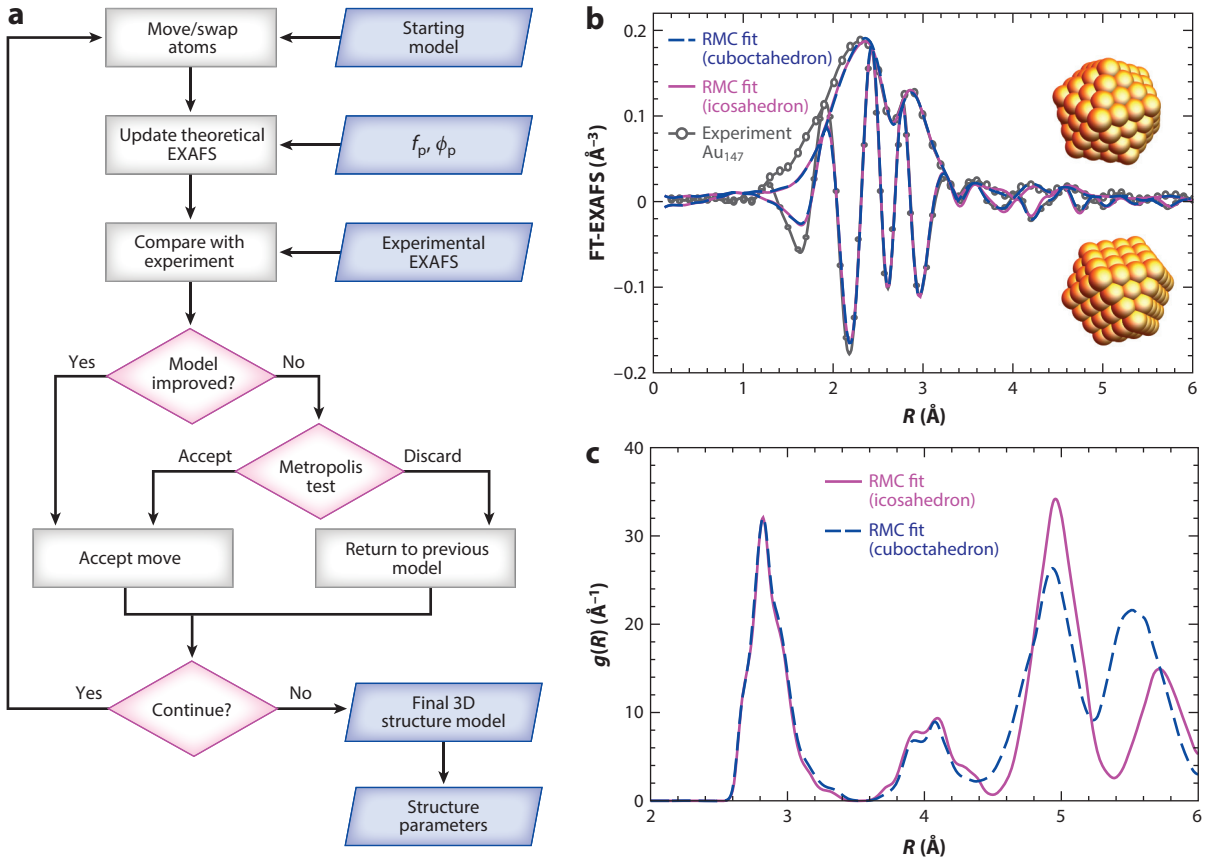

Figure 2

RMC method for analysis of EXAFS data. Flowchart of RMC algorithm for EXAFS data analysis (24, 83) (*a*) and results of RMC fitting for Au L_3-edge EXAFS data for Au_{147} nanoparticles with icosahedral and cuboctahedral starting models: moduli and imaginary values of FTs of experimental and modeled EXAFS (*b*) and RDFs, calculated for final atomic configurations, obtained in RMC simulations (*c*). Panels *b*, *c* adapted with permission from Reference 26. Copyright 2017, Elsevier. Abbreviations: EXAFS, extended X-ray absorption fine structure; FT, Fourier transform; RDF, radial distribution function; RMC, reverse Monte Carlo.

4.2. Reverse Monte Carlo Modeling of Nanoparticle Structure

The obvious difference between RMC analysis of a bulk material and an NP (or a cluster or molecule) is that, in the latter case, the structure model is truncated (e.g., it has a defined surface) and contains a relatively small number of atoms. However, a significantly larger diversity of environments can be expected for nanomaterials because the local structure around atoms, e.g., on the particle surface, can be quite different from that in the NP core. The first case of RMC being used for EXAFS analysis of a truncated system was probably the study by Di Cicco & Trapananti (89), where it was employed to reconstruct the bond-length distribution function in gaseous molecular Br_2. While the simplest possible structure model in this case contains only two atoms, it is not sufficient to reproduce the RDF function because the experimentally measured EXAFS is an average from millions of molecules, each having a slightly different Br–Br distance due to thermal motion. It is clear at this point that an RMC model should represent an ensemble of molecules (or NPs) rather than a single molecule or NP. Therefore, for RMC-EXAFS modeling in this case, a

composite structure model was used, which contained several hundreds of well-separated replicas of the Br_2 molecule (89).

Similarly, if the investigated NPs have fewer than a hundred absorbing atoms, then the structure model for RMC simulations should contain several replicas of the original particle. For example, in a study by Timoshenko et al. (28), RMC was used to analyze EXAFS data from nanosized tungstates (particle size <2 nm). Here, the structure model optimized by RMC simulations involved 64 well-separated particles, each consisting of two metal atoms of each type (e.g., two tungsten atoms and two copper atoms) and the necessary number of oxygen atoms. The possibility of working with a structure model that represents an ensemble of NPs provides interesting opportunities for analysis of heterogeneous samples. In principle, it is not necessary for all of the NP replicas to be the same, and therefore one could envision fitting EXAFS data to more complex models consisting of NPs having different sizes, structures, and/or compositions. The necessary information to construct such model could be available from X-ray diffraction or electron microscopy data (90).

A limitation of the RMC method is that it does not typically allow changes to the total number of atoms in the model. Also, it is most efficient when only relatively small deviations of atoms from their initial positions are allowed, thus preserving the overall topology of the initial structure model. For NPs, this means that the total CNs are imposed in advance by an initial structure model, and they are not refined during the simulations. To circumvent this problem, one may run a series of RMC-EXAFS simulations using different starting models, choosing as the final solution the optimized structure model that resulted in the best agreement with experimental data (28). For example, in a recent study by Kompch et al. (29), such an approach was used for RMC-EXAFS studies of localization of Ag dopant atoms in CdSe nanocrystals.

An important issue with RMC simulations (as with any other method of EXAFS analysis) is the uniqueness of the obtained structure model. First, note that the result of RMC simulations—a set of atomic coordinates—is a product of a random process and, if the calculations are repeated with a different sequence of random moves, the obtained coordinates will be different. In a statistical sense the result of such repeated calculations should be, nevertheless, the same: The RDFs will be the same (within error bars), providing that both RMC procedures resulted in close agreements with experimental data and that experimental data contained sufficient information on the structure parameter of interest. If the information in the experimental data is insufficient, the RMC method may not be able to distinguish between two similar structure models.

An instructive example of the foregoing point is a study by Timoshenko & Frenkel (26), where RMC was used to analyze EXAFS data from Au_{147} NPs. Two structure models were tested as starting structures: one with icosahedral geometry and the other with cuboctahedral geometry. RMC-EXAFS simulations in both cases yielded good agreement with experimental data (see **Figure 2*b***). The inability of the RMC method to discriminate between these two structure models is not surprising: Although these models have quite different structures, the first shell CNs are similar in both cases. Distant coordination shells are more sensitive to the differences between crystallographic structures (69), but owing to disorder effects and a natural dampening of EXAFS contributions at high *R*-values, the contribution of these distant coordination shells is weak. The result, however, cannot be considered a complete failure of the RMC method. First, as shown in **Figure 2*c***, regardless of the starting model, the RDFs yielded by RMC are close and thus can be considered robust model-independent approximations of the true bond-length distribution in Au_{147} NPs. Second, insights from other experimental and theoretical techniques were used to discriminate between structure models that had equally good agreement with experimental EXAFS data. In this specific case, it was known from DFT simulations that the icosahedral structure for

Au_{147} NPs is energetically more favorable, and the bond-length disorder in the icosahedral NPs, as determined by MD simulations, was in better agreement with experimental data (26).

PES: potential energy surface

CMD: classical molecular dynamics

5. DIRECT SIMULATIONS OF EXTENDED X-RAY ABSORPTION FINE STRUCTURE SPECTRA

5.1. Simulations of Static Structure Models

The RMC-EXAFS study of Au_{147} NPs described above shows that it is often impossible to find an unambiguous NP structure model by relying on information from EXAFS data only. Additional information and/or constraints from theoretical simulations are needed. For example, first-principles simulations can be used to restrict the analysis to realistic, energetically plausible structure models. DFT, combined with optimization algorithms, such as simulated annealing (91), the basin hopping method (92–95), and evolutionary (genetic) algorithm methods (96), is commonly used to find NP ground states, which later can be validated with available EXAFS data (19, 20, 97–100). DFT can be used directly either to calculate the energy of a given atomic configuration or to find parameters for an empirical model of the potential energy surface (PES): the total energy of atomic configuration as a function of atomic coordinates $E(\mathbf{r}_1, \mathbf{r}_2, \ldots, \mathbf{r}_n)$. The latter approach is computationally much more efficient, and it allows one to extend NP structure simulations to larger NPs sizes (92, 93, 101–103). However, the design of such empirical potential models is a complex task. The advisability of transferring potentials even between similar systems is still an open question (17). Another problem is the development of potentials for heterogeneous systems, e.g., where metallic phases coexist with oxidized phases, which is a common situation in heterogeneous catalysis (33, 50, 101).

Although CNs, and to some extent interatomic distances, obtained in NP structure optimization can be directly compared with those determined from EXAFS, simulations of static models cannot provide any information on the thermal disorder of the NP. It is not possible, therefore, to use static DFT models for direct EXAFS modeling. In some simple cases, the contribution of thermal disorder to σ_p^2 factors can also be calculated ab initio (104), but these calculations typically rely on the harmonic approximation and are therefore reliable only at low temperatures. More robust approaches to account for disorder effects rely on MD and MC simulations.

5.2. Ab Initio and Classical Molecular Dynamics

In the Born–Oppenheimer approximation, the relatively slow motion of atomic nuclei can be decoupled from the electronic degrees of freedom and, therefore, in many cases, the motion of heavy nuclei can be modeled using classical equations of motion. Knowing the PES function from first-principles simulations [in AIMD] or defined by empirical models [in classical MD (CMD)], one can calculate the forces that act on the i-th atom: $\mathbf{F}_i = -\nabla_{\mathbf{r}_i} E(\mathbf{r}_1, \mathbf{r}_2, \ldots, \mathbf{r}_n)$. Knowledge of forces, in turn, allows one to integrate the Newtonian equations of motion to obtain the trajectories for all atoms in the structure model and to sample the thermal motion of atoms. From such calculations one can thus extract the bond-length distribution, which contains contributions of both the static and thermal disorder. It is important to emphasize here that both in CMD and AIMD the motion of atoms is treated classically, thus neglecting the contribution of quantum effects (zero-point motion). Therefore, special care is needed when MD is applied to simulations at cryogenic temperatures and for light atoms (105, 106).

To validate the MD structure models with EXAFS data, one can either compare the RDF from MD with that obtained from EXAFS data via conventional analysis or, alternatively,

directly compare the experimental and theoretical spectrum calculated for the time-dependent MD model. The former approach has been employed since the 1980s (107). A recent example is the study of cobalt oxide NPs (108), where it was shown that the distances calculated for a dynamical model (obtained using AIMD simulations) are in better agreement with experimental EXAFS than distances calculated using a static DFT model. Similar analysis and comparison of CNs and interatomic distances obtained in MD simulations with EXAFS data were carried out for a cobalt–phosphate catalyst (109). Finally, AIMD-based investigations of the influence of dynamic effects on disorder factors and interatomic distances for supported Pt and PtSn catalysts have been carried out by Rehr, Vila, and colleagues (42, 110, 111).

Direct EXAFS simulations using MD coordinates for interpretation of experimental data were introduced in the 1990s (112), and they allow one to avoid many deficiencies of conventional EXAFS analysis. The MD-EXAFS analysis approach is schematically shown in **Figure 3*a***. To

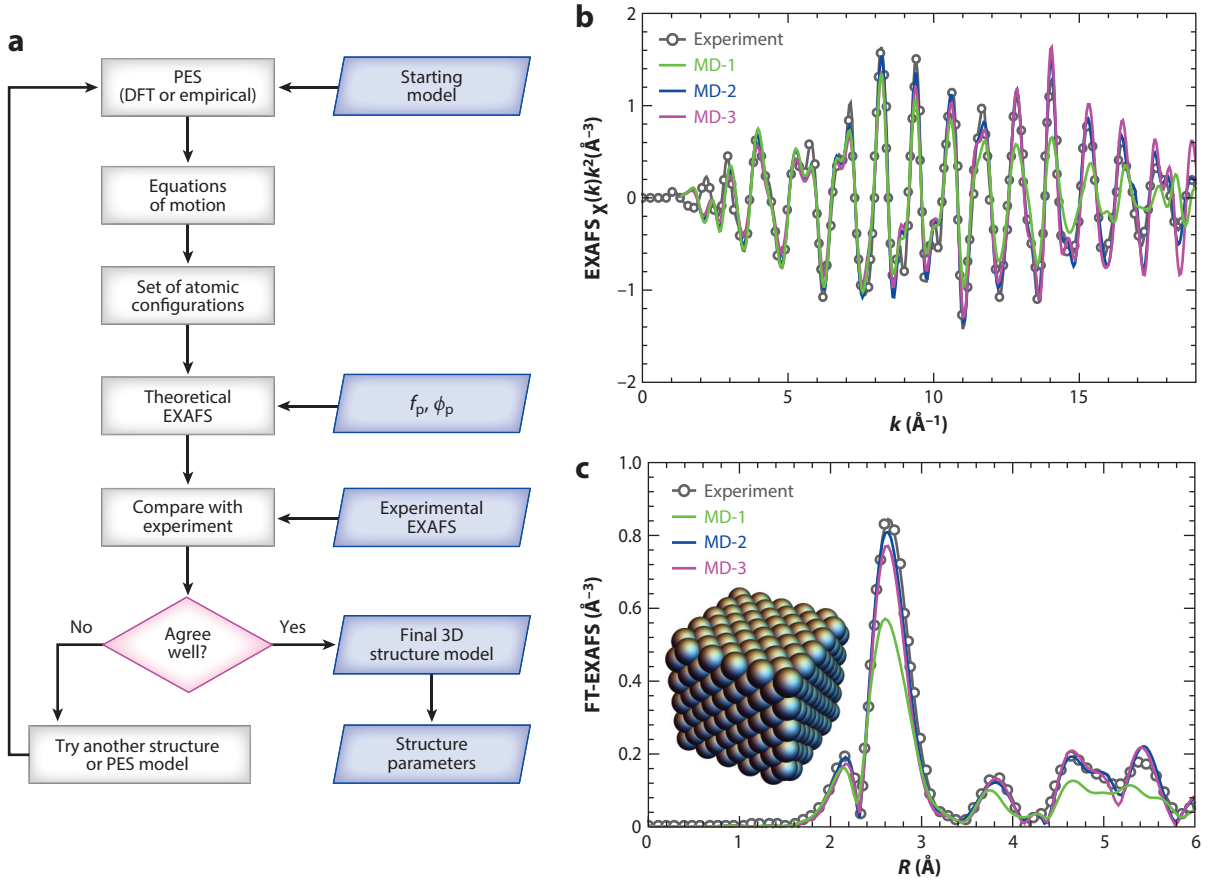

Figure 3

MD method for analysis of EXAFS data. (*a*) Flowchart of MD-EXAFS data analysis algorithm (112, 121) and (*b*) validation of interatomic potentials for bulk Pt: Experimental Pt L_3-edge EXAFS for Pt foil and its FT (*c*) are compared with the results of MD-EXAFS simulations with three different parameterizations of Sutton–Chen potential. One comes from the original work by Sutton & Chen (113) (MD-1), and two more recent versions are from Wen et al. (114) (MD-2) and Vila et al. (33) (MD-3). Inset shows a snapshot of a 5 × 5 × 5 supercell used for simulations. Abbreviations: DFT, density functional theory; EXAFS, extended X-ray absorption fine structure; FT, Fourier transform; MD, molecular dynamics; PES, potential energy surface.

construct MD-EXAFS spectra, one accumulates several hundreds or thousands of MD structure snapshots that capture the atomic positions at different times. For each of the snapshots one then calculates the corresponding theoretical EXAFS. For NP studies it is important to average the calculated spectra over all (or all nonequivalent) atoms in the model. The model-averaged spectra are then averaged over time to obtain theoretical EXAFS spectra that can be directly compared with experimental data (26, 39, 112). In an alternative approach (22), MD coordinates are first used to calculate the RDF, which is then integrated (Equation 2) to obtain the EXAFS spectrum. Although this approach is computationally more efficient, it is limited to analysis of single-scattering contributions only.

Once the MD-EXAFS spectra are calculated and are in good agreement with experimental data, one can claim that the corresponding MD model also closely represents the structure of the investigated sample. Poor agreement can arise from several factors: The initial structure model may be wrong or the chosen PES model does not accurately reflect the interactions in the material. In fact, the sensitivity of EXAFS features to atomic dynamics can be a powerful tool for validating and choosing between different empirical potential models. In **Figure 3*b***, experimental data for bulk Pt are compared with theoretical EXAFS spectra obtained from CMD simulations with three different Sutton–Chen potentials available in the literature (33, 113, 114). Calculations are carried following Timoshenko & Frenkel (26). The positions of the Fourier transform (FT)-EXAFS peaks in all three MD models agree with those in the experimental data, which suggests that interatomic distances are reproduced accurately. However, the model from the original paper by Sutton & Chen (113) fails to reproduce the amplitude of FT-EXAFS features because the thermal motion is overestimated. More recent potential models, however, perform much better and provide almost perfect agreement with experimental data.

Note also that a number of approaches have been proposed to further refine MD models and to improve agreement with experimental data: (*a*) isotropic rescaling of model coordinates to account for systematic errors in interatomic distances (22); (*b*) running MD simulations at a different temperature than the temperature at which the experimental data were collected to account for under- or overestimated atomic vibrations (22, 115); (*c*) refining RDFs via the so-called histogram approach (23, 116) or via fine-tuning the cumulants of bond-length distributions (117, 118); or (*d*) fine-tuning the whole 3D structural model by complementing MD simulations with a consequent RMC run (39). An alternative approach has recently been proposed, where instead of comparing MD-EXAFS spectra directly with experiment, they are used to train an artificial neural network, which is later applied to extract RDF from experimental EXAFS data (119, 120).

One of the first applications of direct EXAFS simulations for NPs using MD methods was the study by Roscioni et al. (22) of gold NPs. MD simulations using Gupta and Sutton–Chen potentials for close-packed NPs with sizes between 2 nm and 6 nm were performed, followed by calculations of EXAFS spectra. It was found that MD simulations can reproduce the experimental data at room temperature. Although the employed potential models were optimized to reproduce bulk properties of gold, MD simulations of NPs were able to account for the asymmetry of bond-length distributions and, at least qualitatively, for structure relaxation due to surface tension. The surface compression, however, was underestimated in MD models, while the thermal disorder was overestimated at high temperatures. These inaccuracies in the details of bond-length distribution are not surprising considering the simplicity of the interaction model employed. MD simulations of gold NPs with Sutton–Chen potential were recently revisited by Timoshenko & Frenkel (26), with the important difference that, in this latter study, the contribution of multiple-scattering effects to EXAFS spectra was also modeled and found to be in good agreement with experimental data (**Figure 4**).

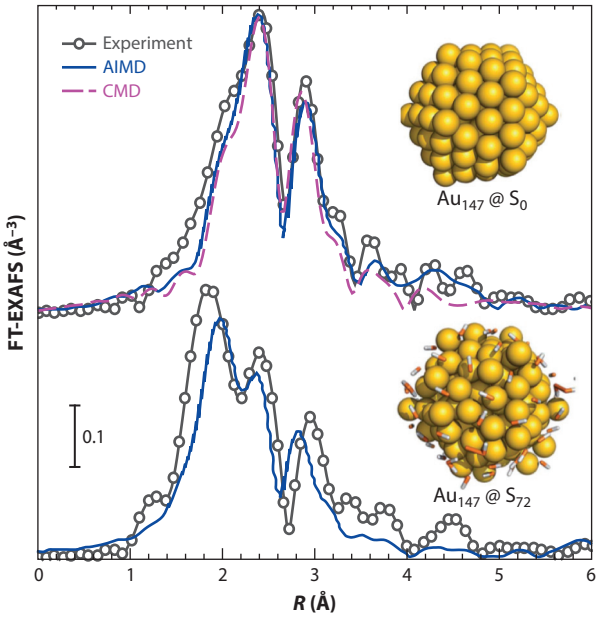

Figure 4

CMD and AIMD for analysis of EXAFS data in Au_{147} nanoparticles. Both CMD (26) and AIMD (18) can be successfully used to reproduce EXAFS spectra of bare Au_{147} nanoparticles. The AIMD method, however, is required to properly account for interactions with ligands. Corresponding structure models of bare nanoparticles and nanoparticles covered with 72 thiol molecules are shown in the insets. Insets adapted with permission from Reference 18. Copyright 2013, Royal Society of Chemistry. Abbreviations: AIMD, ab initio molecular dynamics; CMD, classical molecular dynamics; EXAFS, extended X-ray absorption fine structure; FT, Fourier transform.

The usefulness of MD-EXAFS analysis for distinguishing between NPs of different sizes, structures and compositions was recently demonstrated by Timoshenko et al. (39) in the study of PdAu nanoparticles. Here, MD simulations based on Sutton–Chen potential were carried out for a large set of NP models with different numbers of atoms, different atomic packings, and different concentrations and locations of Au and Pd atoms (random distribution versus core shell–type structure motifs). All of these differences had a pronounced effect on the simulated spectra. By directly matching the simulated MD-EXAFS spectra with the experimental Pd K-edge and Au L_3-edge EXAFS data, it was possible to identify the most likely structure models for the investigated NPs (39).

For nonmetallic NPs, a similar MD-EXAFS method was applied by Anspoks and coworkers (64, 122–125). In these studies, simulations of nickel K-edge EXAFS spectra for cubic nickel oxide NPs with different sizes and concentrations of oxygen vacancies were performed using MD simulations with a Buckingham-type force-field model (126). Simulated spectra were then compared with experimental data, making it possible to identify the most likely structure model (i.e., NP size and vacancy concentration) and to investigate structure relaxation around oxygen vacancies. Importantly, it was found that the calculations of contributions of distant coordination shells and multiple-scattering effects are essential because information from the first two single-scattering paths was insufficient to find an unambiguous structure model. This study is also one of very few examples where experimental EXAFS data are used to refine the details of an empirical potential model.

AIMD requires significantly more computational resources than CMD, and therefore it is relatively rarely employed for simulations of dynamical effects in EXAFS spectra. Among the successful examples, we mention the study by Yancey et al. (18). Simulations of Au_{147} NPs covered with different numbers of thiol ligands were performed, followed by calculation of time- and configuration-averaged EXAFS spectra, which were directly compared with experimental EXAFS data for gold NPs synthesized using a dendrimer encapsulation method. It was found that increasing the number of ligands systematically increases the disorder in the NP and that this trend can be reproduced well by MD simulations. As shown in **Figure 4**, for bare Au_{147} particles the accuracy of AIMD-EXAFS is comparable with that of the classical MD-EXAFS method. The advantage of AIMD is most clearly observed when modeling heterogeneous environments of absorbing atoms (e.g., when interactions with ligands are important). Another case where the use of AIMD is required is when systems with complex bonding motifs or highly fluxional systems are considered. In these cases, the bond formation and dissociation processes must be addressed. In one relevant example, Rousseau et al. (127) considered a homogeneous Rh_4 catalyst, and AIMD was used to validate the resulting structure model. Another recent example is a study by Chen et al. (128) of cobalt oxide NPs, where AIMD and comparison of simulated spectra with experimental data were employed to identify the likely morphology of these NPs.

5.3. Monte Carlo Simulations for Extended X-Ray Absorption Fine Structure Data Interpretation

The structure snapshots required for EXAFS simulations can also be obtained using the MC method. The same Metropolis algorithm is used here, as introduced in Section 4. The cost function Δ in this case is the total energy $\Delta = E/k_B$ (obtained from empirical potential model or DFT calculations). The scaling parameter T is directly interpreted as temperature. By performing random moves that are accepted or discarded based on the Metropolis criterion, the atomic configurations will be sampled with a probability proportional to e^{-E/k_BT} (84, 129). Thus, if for each of the configurations some structure-dependent property [e.g., configuration-averaged EXAFS (130, 131)] is calculated and averaged, the averaged property will correspond to the expected value in the canonical ensemble with temperature T; i.e., it will be equivalent to the one obtained in MD simulations. However, MC typically requires a much larger number of iterations to obtain a representative set of structure snapshots.

For EXAFS data interpretation, MC simulations with empirical potential were recently employed by Duan and coworkers (38, 41) to simulate EXAFS spectra in a heterogeneous system consisting of a mixture of pure Rh particles and bimetallic RhAu nanoparticles. Another MC-related approach for simulation of EXAFS spectra was proposed by Duan and colleagues (32, 44) for simulations of Au and Au Pt nanoparticles. In this case, DFT simulations were used to calculate a dynamical matrix and derive from it harmonic force constants and normal vibrational modes. Structure snapshots were then generated by independent displacement of atoms along each normal mode. The displacement magnitude was sampled from a Gaussian distribution with the variance corresponding to the position variance of a quantum harmonic oscillator (with vibrational frequencies corresponding to the eigenvalues of the dynamical matrix). This approach also allows one to obtain good agreement between simulated and experimental EXAFS data, while providing more direct access to vibrational properties of the material (32).

6. OTHER EXPERIMENTAL TECHNIQUES

Although we have focused on the analysis of EXAFS data, the approaches discussed here can be helpful for interpretation of other structure-sensitive experimental data. For example, they can be

applied in a similar way for interpretation of X-ray absorption near-edge structure (XANES) data. Like EXAFS, XANES also contains information on the local environment of absorbing atoms, but it is more sensitive to the electronic state of the absorber. Therefore, it can be used to identify changes in the valence state or symmetry of the absorbing site environment (132) and to probe the charge transfer between NPs, supports, and adsorbates (133, 134). Analysis based on constructing 3D NP structure models is especially attractive for XANES because path-by-path approaches are not applicable in this spectral region. Like EXAFS, XANES data can also be used to validate DFT-generated 3D structure models (135, 136). Likewise, the influence of atomic thermal motion on XANES spectra can be modeled by MD simulations (111, 137).

XANES: X-ray absorption near-edge structure

There are also many examples where MD and RMC methods are used to assist in the interpretation of X-ray or neutron total scattering data (PDF analysis). For instance, Naicker et al. (138) used CMD simulations for interpreting powder diffraction patterns of titanium dioxide NPs. Yamamoto et al. (139) recently used the RMC technique to interpret X-ray scattering data for silver iodide NPs. To interpret PDF data, Petkov and coworkers (17, 51) used MD simulations followed by hybrid-RMC fine-tuning for a study of metal NPs and RMC simulations for a study of silicon (140) and ruthenium (141) NPs. For heterometallic NPs, a promising approach is to rely on the resonant X-ray total scattering technique, which combines sensitivity to medium-range order, as in conventional scattering experiments, with element specificity, as in XAS. MD and/or RMC simulations can then be used to find a 3D structure model, consistent with the partial pair distribution functions, extracted from scattering data collected at different absorption edges (142, 143). MD simulations were found to be useful even in the interpretation of electron microscopy data (144).

One strength of using atomistic simulations for the interpretation of XAS (and other) data is that the final results are formulated directly in terms of universal structure motifs, rather than method-specific descriptors of NP structure (such as average interatomic distance and disorder factors). The findings of such analysis can thus immediately be correlated with results yielded by other structure-sensitive techniques. It also means that the data from complementary methods can be used to further constrain analysis and to construct a single structure model that agrees with all available experimental information. For example, it is very common to combine EXAFS and PDF data in RMC simulations (145). This can be ensured by defining the cost function for RMC simulations as $\Delta = \sum_{\xi} w_{\xi} \Delta_{\xi}$, where Δ_{ξ} are cost functions associated with different experimental data weighted with weights w_{ξ}. In some cases, a less direct combination of scattering and EXAFS analysis is more efficient. For example, in some studies (30, 36), partial CNs obtained from EXAFS analysis of PdAu NPs were used to constrain structure models and refined further by RMC simulations of PDF patterns (which themselves are not sensitive to the differences between types of atoms).

SUMMARY POINTS

1. EXAFS spectroscopy is a powerful method to probe the structure of NPs, but the data analysis is prone to artifacts, and the interpretation of obtained results is often problematic. A combination of experimental data analysis with modeling of atomistic structures can be used to address this issue.
2. Some of the challenges associated with the conventional approaches for EXAFS analysis are the result of complex, asymmetric bond-length distributions, often present in

NPs, and an overlap of contributions from different coordination shells and multiple-scattering effects. These issues can be addressed with RMC methods.

3. Often the experimental data alone do not contain sufficient information to recover the 3D structure model of a NP unambiguously. In this case input from first-principles simulations of the structure and dynamics of NPs using the DFT approach, and/or an empirical model of interatomic interactions, can assist in the interpretation of experimental data, while structure-sensitive information, encoded in EXAFS, can be used to validate theoretical structure models.
4. Atomistic simulations allow one to reconcile the structural information, accessible by various experimental techniques, and provided by theoretical simulations. The obtained 3D structure models can be used directly in first-principles simulations of the electronic, optical, chemical and catalytic properties of materials, thereby enabling direct correlation of material structure and function.

DISCLOSURE STATEMENT

The authors are not aware of any affiliations, memberships, funding, or financial holdings that might be perceived as affecting the objectivity of this review.

ACKNOWLEDGMENTS

A.I.F., G.H., and R.M.C. gratefully acknowledge support from the Catalysis Science Program, Chemical Sciences, Geosciences, and Biosciences Division, Office of Basic Energy Sciences, Office of Science, US Department of Energy (contract DE-FG02–13ER15476 to A.I.F. and contract DE-SC0010576 to G.H. and R.M.C.). R.M.C. thanks the Robert A. Welch Foundation (grant F-0032) for sustaining resources.

LITERATURE CITED

1. Mostafa S, Behafarid F, Croy JR, Ono LK, Li L, et al. 2010. Shape-dependent catalytic properties of Pt nanoparticles. *J. Am. Chem. Soc.* 132:15714–19
2. Guliamov O, Frenkel AI, Menard LD, Nuzzo RG, Kronik L. 2007. Tangential ligand-induced strain in icosahedral Au_{13}. *J. Am. Chem. Soc.* 129:10978–79
3. Zhang L, Henkelman G. 2014. Computational design of alloy-core@shell metal nanoparticle catalysts. *ACS Catal.* 5:655–60
4. Choi Y-W, Mistry H, Roldan Cuenya B. 2017. New insights into working nanostructured electrocatalysts through operando spectroscopy and microscopy. *Curr. Opin. Electrochem.* 1:95–103
5. Behafarid F, Roldan Cuenya B. 2013. Towards the understanding of sintering phenomena at the nanoscale: geometric and environmental effects. *Top. Catal.* 56:1542–59
6. Billinge SJL, Levin I. 2007. The problem with determining atomic structure at the nanoscale. *Science* 316:561–65
7. Rehr JJ, Albers RC. 2000. Theoretical approaches to X-ray absorption fine structure. *Rev. Mod. Phys.* 72:621–54
8. Sayers DE, Stern EA, Lytle FW. 1971. New technique for investigating noncrystalline structures: Fourier analysis of the extended X-ray–absorption fine structure. *Phys. Rev. Lett.* 27:1204
9. Stern E. 1988. Theory of EXAFS. In *X-Ray Absorption: Principles, Applications, Techniques of EXAFS, SEXAFS, and XANES*, ed. D Koningsberger, R Prins, pp. 3–52. New York: John Wiley & Sons

10. Frenkel AI, Yevick A, Cooper C, Vasic R. 2011. Modeling the structure and composition of nanoparticles by extended X-ray absorption fine-structure spectroscopy. *Annu. Rev. Anal. Chem.* 4:23–39
11. Frenkel AI. 2012. Applications of extended X-ray absorption fine-structure spectroscopy to studies of bimetallic nanoparticle catalysts. *Chem. Soc. Rev.* 41:8163–78
12. Sinfelt J, Via G, Lytle F. 1984. Application of EXAFS in catalysis. Structure of bimetallic cluster catalysts. *Catal. Rev. Sci. Eng.* 26:81–140
13. Yevick A, Frenkel AI. 2010. Effects of surface disorder on EXAFS modeling of metallic clusters. *Phys. Rev. B* 81:115451
14. Hansen LB, Stoltze P, Nørskov JK, Clausen B, Niemann W. 1990. Is there a contraction of the interatomic distance in small metal particles? *Phys. Rev. Lett.* 64:3155
15. Chill ST, Anderson RM, Yancey DF, Frenkel AI, Crooks RM, Henkelman G. 2015. Probing the limits of conventional extended X-ray absorption fine structure analysis using thiolated gold nanoparticles. *ACS Nano* 9:4036–42
16. Stern EA, Ma Y, Hanske-Petitpierre O, Bouldin CE. 1992. Radial distribution function in X-ray-absorption fine structure. *Phys. Rev. B* 46:687–94
17. Prasai B, Wilson A, Wiley B, Ren Y, Petkov V. 2015. On the road to metallic nanoparticles by rational design: bridging the gap between atomic-level theoretical modeling and reality by total scattering experiments. *Nanoscale* 7:17902–22
18. Yancey DF, Chill ST, Zhang L, Frenkel AI, Henkelman G, Crooks RM. 2013. A theoretical and experimental examination of systematic ligand-induced disorder in Au dendrimer-encapsulated nanoparticles. *Chem. Sci.* 4:2912–21
19. Anderson RM, Yancey DF, Zhang L, Chill ST, Henkelman G, Crooks RM. 2015. A theoretical and experimental approach for correlating nanoparticle structure and electrocatalytic activity. *Acc. Chem. Res.* 48:1351–57
20. Anderson RM, Zhang L, Loussaert JA, Frenkel AI, Henkelman G, Crooks RM. 2013. An experimental and theoretical investigation of the inversion of Pd@Pt core@shell dendrimer-encapsulated nanoparticles. *ACS Nano* 7:9345–53
21. Di Cicco A, Minicucci M, Principi E, Witkowska A, Rybicki J, Laskowski R. 2002. Testing interaction models by using X-ray absorption spectroscopy: solid Pb. *J. Phys. Condens. Matter* 14:3365
22. Roscioni OM, Zonias N, Price SW, Russell AE, Comaschi T, Skylaris C-K. 2011. Computational prediction of L_3 EXAFS spectra of gold nanoparticles from classical molecular dynamics simulations. *Phys. Rev. B* 83:115409
23. Price SW, Zonias N, Skylaris C-K, Hyde TI, Ravel B, Russell AE. 2012. Fitting EXAFS data using molecular dynamics outputs and a histogram approach. *Phys. Rev. B* 85:075439
24. Gurman S, McGreevy R. 1990. Reverse Monte Carlo simulation for the analysis of EXAFS data. *J. Phys. Condens. Matter* 2:9463
25. Timoshenko J, Kuzmin A, Purans J. 2014. EXAFS study of hydrogen intercalation into ReO_3 using the evolutionary algorithm. *J. Phys. Condens. Matter* 26:055401
26. Timoshenko J, Frenkel AI. 2017. Probing structural relaxation in nanosized catalysts by combining EXAFS and reverse Monte Carlo methods. *Catal. Today* 280:274–82
27. Opletal G, Petersen T, O'Malley B, Snook I, McCulloch DG, et al. 2002. Hybrid approach for generating realistic amorphous carbon structure using metropolis and reverse Monte Carlo. *Mol. Simul.* 28:927–38
28. Timoshenko J, Anspoks A, Kalinko A, Kuzmin A. 2015. Local structure of nanosized tungstates revealed by evolutionary algorithm. *Phys. Status Solidi A* 212:265–73
29. Kompch A, Sahu A, Notthoff C, Ott F, Norris DJ, Winterer M. 2015. Localization of Ag dopant atoms in CdSe nanocrystals by reverse Monte Carlo analysis of EXAFS spectra. *J. Phys. Chem. C* 119:18762–72
30. Merrill NA, McKee EM, Merino KC, Drummy LF, Lee S, et al. 2015. Identifying the atomic-level effects of metal composition on the structure and catalytic activity of peptide-templated materials. *ACS Nano* 9:11968–79

31. Timoshenko J, Shivhare A, Scott RWJ, Lu DY, Frenkel AI. 2016. Solving local structure around dopants in metal nanoparticles with ab initio modeling of X-ray absorption near edge structure. *Phys. Chem. Chem. Phys.* 18:19621–30
32. Duan Z, Li Y, Timoshenko J, Chill ST, Anderson RM, et al. 2016. A combined theoretical and experimental EXAFS study of the structure and dynamics of Au_{147} nanoparticles. *Catal. Sci. Technol.* 6:6879–85
33. Vila FD, Hayashi ST, Moore JM, Rehr JJ. 2016. Molecular dynamics simulations of supported Pt nanoparticles with a hybrid Sutton–Chen potential. *J. Phys. Chem. C* 120:14883–91
34. Avakyan L, Srabionyan V, Pryadchenko V, Bulat N, Bugaev L. 2016. Construction of three-dimensional models of bimetallic nanoparticles based on X-ray absorption spectroscopy data. *Opt. Spectrosc.* 120:926–32
35. Jonane I, Lazdins K, Timoshenko J, Kuzmin A, Purans J, et al. 2016. Temperature-dependent EXAFS study of the local structure and lattice dynamics in cubic Y_2O_3. *J. Synchrotron Radiat.* 23:510–18
36. Bedford NM, Showalter AR, Woehl TJ, Hughes ZE, Lee S, et al. 2016. Peptide-directed PdAu nanoscale surface segregation: toward controlled bimetallic architecture for catalytic materials. *ACS Nano* 10:8645–59
37. Bugaev AL, Guda AA, Lazzarini A, Lomachenko KA, Groppo E, et al. 2017. In situ formation of hydrides and carbides in palladium catalyst: when XANES is better than EXAFS and XRD. *Catal. Today* 283:119–26
38. House SD, Bonifacio CS, Timoshenko J, Kunal P, Wan H, et al. 2017. Computationally assisted STEM and EXAFS characterization of tunable Rh/Au and Rh/Ag bimetallic nanoparticle catalysts. *Microsc. Microanal.* 23:2030–31
39. Timoshenko J, Keller KR, Frenkel AI. 2017. Determination of bimetallic architectures in nanometer-scale catalysts by combining molecular dynamics simulations with X-ray absorption spectroscopy. *J. Chem. Phys.* 146:114201
40. Timoshenko J, Lu D, Lin Y, Frenkel AI. 2017. Supervised machine learning-based determination of three-dimensional structure of metallic nanoparticles. *J. Phys. Chem. Lett.* 23:510–18
41. Duan Z, Timoshenko J, Kunal P, House SD, Wan H, et al. 2018. Structural characterization on heterogeneous RhAu nanoparticles from a microwave-assisted synthesis. *Nanoscale* 10:22520–32
42. Vila FD, Rehr JJ, Nuzzo RG, Frenkel AI. 2017. Anomalous structural disorder in supported Pt nanoparticles. *J. Phys. Chem. Lett.* 8:3284–88
43. Luo L, Timoshenko J, Lapp AS, Frenkel AI, Crooks RM. 2017. Structural characterization of Rh and RhAu dendrimer-encapsulated nanoparticles. *Langmuir* 33:12434–42
44. Lapp AS, Duan Z, Marcella N, Luo L, Genc A, et al. 2018. Experimental and theoretical structural investigation of AuPt nanoparticles synthesized using a direct electrochemical method. *J. Am. Chem. Soc.* 140:6249–59
45. Di Cicco A, Iesari F, Trapananti A, D'Angelo P, Filipponi A. 2018. Structure and atomic correlations in molecular systems probed by XAS reverse Monte Carlo refinement. *J. Chem. Phys.* 148:094307
46. Ankudinov AL, Ravel B, Rehr JJ, Conradson SD. 1998. Real-space multiple-scattering calculation and interpretation of X-ray-absorption near-edge structure. *Phys. Rev. B* 58:7565–76
47. Frenkel AI. 1999. Solving the structure of nanoparticles by multiple-scattering EXAFS analysis. *J. Synchrotron Radiat.* 6:293–95
48. Frenkel A. 2007. Solving the 3D structure of metal nanoparticles. *Z. Kristallogr.* 222:605–11
49. Huang W, Sun R, Tao J, Menard L, Nuzzo R, Zuo J. 2008. Coordination-dependent surface atomic contraction in nanocrystals revealed by coherent diffraction. *Nat. Mater.* 7:308–13
50. Lei Y, Zhao H, Rivas RD, Lee S, Liu B, et al. 2014. Adsorbate-induced structural changes in 1–3 nm platinum nanoparticles. *J. Am. Chem. Soc.* 136:9320–26
51. Petkov V, Prasai B, Ren Y, Shan S, Luo J, et al. 2014. Solving the nanostructure problem: exemplified on metallic alloy nanoparticles. *Nanoscale* 6:10048–61
52. Clausen BS, Nørskov JK. 2000. Asymmetric pair distribution functions in catalysts. *Top. Catal.* 10:221–30
53. Clausen BS, Topsøe H, Hansen LB, Stoltze P, Nørskov JK. 1993. The effect of anharmonicity on the EXAFS coordination number in small metallic particles. *Jpn. J. Appl. Phys.* 32:95

54. Clausen B, Topsøe H, Hansen L, Stoltze P, Nørskov J. 1994. Determination of metal particle sizes from EXAFS. *Catal. Today* 21:49–55
55. Clausen B, Grabaek L, Topsøe H, Hansen L, Stoltze P, et al. 1993. A new procedure for particle size determination by EXAFS based on molecular dynamics simulations. *J. Catal.* 141:368–79
56. Mierzwa B. 2004. EXAFS as a tool for studies of bimetallic PdCo nanocluster structure. *J. Alloys Compd.* 362:178–88
57. Mierzwa B. 2005. EXAFS studies of bimetallic palladium–cobalt nanoclusters using Molecular Dynamics simulations. *J. Alloys Compd.* 401:127–34
58. Frenkel A, Rehr J. 1993. Thermal expansion and X-ray-absorption fine-structure cumulants. *Phys. Rev. B* 48:585
59. Dalba G, Fornasini P. 1997. EXAFS Debye–Waller factor and thermal vibrations of crystals. *J. Synchrotron Radiat.* 4:243–55
60. Witkowska A, Di Cicco A, Principi E. 2007. Local ordering of nanostructured Pt probed by multiple-scattering XAFS. *Phys. Rev. B* 76:104110
61. Filipponi A. 2001. EXAFS for liquids. *J. Phys. Condens. Matter* 13:R23
62. Gilbert B, Zhang H, Huang F, Banfield JF, Ren Y, et al. 2004. Analysis and simulation of the structure of nanoparticles that undergo a surface-driven structural transformation. *J. Chem. Phys.* 120:11785–95
63. Crozier ED, Rehr JJ, Ingalls R. 1988. Amorphous and liquid systems. In *X-Ray Absorption: Principles, Applications, Techniques of EXAFS, SEXAFS, and XANES*, ed. D Koningsberger, R Prins, pp. 373–442. New York: John Wiley & Sons
64. Kuzmin A, Chaboy J. 2014. EXAFS and XANES analysis of oxides at the nanoscale. *IUCrJ* 1:571–89
65. Bordiga S, Groppo E, Agostini G, van Bokhoven JA, Lamberti C. 2013. Reactivity of surface species in heterogeneous catalysts probed by in situ X-ray absorption techniques. *Chem. Rev.* 113:1736–850
66. Frenkel A, Stern E, Voronel A, Qian M, Newville M. 1993. Buckled crystalline structure of mixed ionic salts. *Phys. Rev. Lett.* 71:3485
67. Teo BK. 1986. Data analysis in practice. In *EXAFS: Basic Principles and Data Analysis*, ed. BK Teo, pp. 114–57. Berlin/Heidelberg: Springer
68. Kuzmin A, Purans J. 1993. The influence of the focusing effect on the X-ray absorption fine structure above all the tungsten L edges in non-stoichiometric tungsten oxides. *J. Phys. Condens. Matter* 5:9423
69. Glasner D, Frenkel AI. 2007. Geometrical characteristics of regular polyhedra: application to EXAFS studies of nanoclusters. *AIP Conf. Proc.* 882:746–48
70. Frenkel AI, Frankel SC, Liu T. 2005. Structural stability of giant polyoxomolybdate molecules as probed by EXAFS. *Phys. Scr.* 2005:721
71. Agostini G, Piovano A, Bertinetti L, Pellegrini R, Leofanti G, et al. 2014. Effect of different face centered cubic nanoparticle distributions on particle size and surface area determination: a theoretical study. *J. Phys. Chem. C* 118:4085–94
72. Foster D, Ferrando R, Palmer R. 2018. Experimental determination of the energy difference between competing isomers of deposited, size-selected gold nanoclusters. *Nat. Commun.* 9:1323
73. Li Y, Zakharov D, Zhao S, Tappero R, Jung U, et al. 2015. Complex structural dynamics of nanocatalysts revealed in *Operando* conditions by correlated imaging and spectroscopy probes. *Nat. Commun.* 6:7583
74. Myers VS, Weir MG, Carino EV, Yancey DF, Pande S, Crooks RM. 2011. Dendrimer-encapsulated nanoparticles: new synthetic and characterization methods and catalytic applications. *Chem. Sci.* 2:1632–46
75. Crooks RM, Zhao M, Sun L, Chechik V, Yeung LK. 2001. Dendrimer-encapsulated metal nanoparticles: synthesis, characterization, and applications to catalysis. *Acc. Chem. Res.* 34:181–90
76. Niu Y, Crooks RM. 2003. Dendrimer-encapsulated metal nanoparticles and their applications to catalysis. *Comptes Rendus Chim.* 6:1049–59
77. Roldan Cuenya B, Croy JR, Mostafa S, Behafarid F, Li L, et al. 2010. Solving the structure of size-selected Pt nanocatalysts synthesized by inverse micelle encapsulation. *J. Am. Chem. Soc.* 132:8747–56
78. Jakhmola A, Bhandari R, Pacardo DB, Knecht MR. 2010. Peptide template effects for the synthesis and catalytic application of Pd nanoparticle networks. *J. Mater. Chem.* 20:1522–31

79. Nykypanchuk D, Maye MM, Van Der Lelie D, Gang O. 2008. DNA-guided crystallization of colloidal nanoparticles. *Nature* 451:549–52
80. McGreevy R, Pusztai L. 1988. Reverse Monte Carlo simulation: a new technique for the determination of disordered structures. *Mol. Simul.* 1:359–67
81. McGreevy RL. 2001. Reverse Monte Carlo modelling. *J. Phys. Condens. Matter* 13:R877
82. Tupy SA, Karim AM, Bagia C, Deng W, Huang Y, et al. 2012. Correlating ethylene glycol reforming activity with in situ EXAFS detection of Ni segregation in supported NiPt bimetallic catalysts. *ACS Catal.* 2:2290–96
83. Timoshenko J, Kuzmin A, Purans J. 2012. Reverse Monte Carlo modeling of thermal disorder in crystalline materials from EXAFS spectra. *Comp. Phys. Commun.* 183:1237–45
84. Metropolis N, Rosenbluth AW, Rosenbluth MN, Teller AH, Teller E. 1953. Equation of state calculations by fast computing machines. *J. Chem. Phys.* 21:1087–92
85. Timoshenko J, Anspoks A, Kalinko A, Kuzmin A. 2017. Thermal disorder and correlation effects in anti-perovskite-type copper nitride. *Acta Mater.* 129:61–71
86. McGreevy R, Howe M. 1992. RMC: modeling disordered structures. *Annu. Rev. Mater. Sci.* 22:217–42
87. Tucker MG, Keen DA, Dove MT, Goodwin AL, Hui Q. 2007. RMCProfile: reverse Monte Carlo for polycrystalline materials. *J. Phys. Condens. Matter* 19:335218
88. Pethes I, Pusztai L. 2017. Reverse Monte Carlo modeling of liquid water with the explicit use of the SPC/E interatomic potential. *J. Chem. Phys.* 146:064506
89. Di Cicco A, Trapananti A. 2005. Reverse Monte Carlo refinement of molecular and condensed systems by X-ray absorption spectroscopy. *J. Phys. Condens. Matter* 17:S135
90. Sestu M, Navarra G, Carrero S, Valvidares S, Aquilanti G, et al. 2017. Whole-nanoparticle atomistic modeling of the schwertmannite structure from total scattering data. *J. Appl. Crystallogr.* 50:1617–26
91. Kirkpatrick S, Gelatt CD, Vecchi MP. 1983. Optimization by simulated annealing. *Science* 220:671–80
92. Ferrando R. 2012. Computational methods for predicting the structures of nanoalloys. In *Nanoalloys*, ed. D Alloyeau, C Mottet, C Ricolleau, pp. 259–86. London: Springer
93. Ferrando R, Jellinek J, Johnston RL. 2008. Nanoalloys: from theory to applications of alloy clusters and nanoparticles. *Chem. Rev.* 108:845–910
94. Wales DJ, Scheraga HA. 1999. Global optimization of clusters, crystals, and biomolecules. *Science* 285:1368–72
95. Yu W-Y, Zhang L, Mullen GM, Evans EJ, Henkelman G, Mullins CB. 2015. Effect of annealing in oxygen on alloy structures of Pd–Au bimetallic model catalysts. *Phys. Chem. Chem. Phys.* 17:20588–96
96. Holland JH. 1992. *Adaptation in Natural and Artificial Systems: An Introductory Analysis with Applications to Biology, Control, and Artificial Intelligence*. Cambridge, MA: MIT Press
97. Wang L-L, Johnson D. 2007. Shear instabilities in metallic nanoparticles: hydrogen-stabilized structure of Pt_{37} on carbon. *J. Am. Chem. Soc.* 129:3658–64
98. Wang L-L, Khare SV, Chirita V, Johnson DD, Rockett AA, et al. 2006. Origin of bulklike structure and bond length disorder of Pt_{37} and Pt_6Ru_{31} clusters on carbon: comparison of theory and experiment. *J. Am. Chem. Soc.* 128:131–42
99. Kang JH, Menard LD, Nuzzo RG, Frenkel AI. 2006. Unusual non-bulk properties in nanoscale materials: thermal metal–metal bond contraction of γ-alumina-supported Pt catalysts. *J. Am. Chem. Soc.* 128:12068–69
100. Bromley S, Sankar G, Catlow C, Maschmeyer T, Johnson B, Thomas J. 2001. New insights into the structure of supported bimetallic nanocluster catalysts prepared from carbonylated precursors: a combined density functional theory and EXAFS study. *Chem. Phys. Lett.* 340:524–30
101. Mora-Fonz D, Lazauskas T, Woodley SM, Bromley ST, Catlow CRA, Sokol AA. 2017. Development of interatomic potentials for supported nanoparticles: the Cu/ZnO case. *J. Phys. Chem. C* 121:16831–44
102. Shao G-F, Tu N-N, Liu T-D, Xu L-Y, Wen Y-H. 2015. Structural studies of Au–Pd bimetallic nanoparticles by a genetic algorithm method. *Phys. E Low-Dimens. Syst. Nanostructures* 70:11–20

103. Pittaway F, Paz-Borbón LO, Johnston RL, Arslan H, Ferrando R, et al. 2009. Theoretical studies of palladium–gold nanoclusters: Pd–Au clusters with up to 50 atoms. *J. Phys. Chem. C* 113:9141–52
104. Vila FD, Rehr J, Rossner H, Krappe H. 2007. Theoretical X-ray absorption Debye-Waller factors. *Phys. Rev. B* 76:014301
105. Berne BJ, Thirumalai D. 1986. On the simulation of quantum systems: path integral methods. *Annu. Rev. Phys. Chem.* 37:401–24
106. Beccara S, Dalba G, Fornasini P, Grisenti R, Pederiva F, et al. 2003. Local thermal expansion in copper: extended X-ray-absorption fine-structure measurements and path-integral Monte Carlo calculations. *Phys. Rev. B* 68:140301
107. Hayes T, Boyce J. 1980. EXAFS as a probe of atom-atom interaction potentials: AgI and CuI. *J. Phys. C Solid State Phys.* 13:L731
108. Aksoy Akgul F, Akgul G, Kurban M. 2016. Microstructural properties and local atomic structures of cobalt oxide nanoparticles synthesised by mechanical ball-milling process. *Philos. Mag.* 96:3211–26
109. Hu XL, Piccinin S, Laio A, Fabris S. 2012. Atomistic structure of cobalt-phosphate nanoparticles for catalytic water oxidation. *ACS Nano* 6:10497–504
110. Rehr J, Vila F. 2014. Dynamic structural disorder in supported nanoscale catalysts. *J. Chem. Phys.* 140:134701
111. Vila F, Rehr J, Kas J, Nuzzo R, Frenkel A. 2008. Dynamic structure in supported Pt nanoclusters: real-time density functional theory and X-ray spectroscopy simulations. *Phys. Rev. B* 78:121404
112. Palmer BJ, Pfund DM, Fulton JL. 1996. Direct modeling of EXAFS spectra from molecular dynamics simulations. *J. Phys. Chem.* 100:13393–98
113. Sutton A, Chen J. 1990. Long-range Finnis–Sinclair potentials. *Philos. Mag. Lett.* 61:139–46
114. Wen Y, Fang H, Zhu Z, Sun S. 2009. Molecular dynamics investigation of shape effects on thermal characteristics of platinum nanoparticles. *Phys. Lett. A* 373:272–76
115. Timoshenko J, Kuzmin A, Purans J. 2011. Molecular dynamics simulations of EXAFS in germanium. *Cent. Eur. J. Phys.* 9:710–15
116. Price SW, Zonias N, Skylaris C-K, Russell AE, Ravel B. 2013. The application of molecular dynamics to fitting EXAFS data. *J. Phys. Conf. Ser.* 430:0120009
117. Binsted N, Edwards A, Evans J, Weller M. 2005. The mean square variation of multiple scattering path length by molecular dynamics simulation. *Phys. Scr.* 2005:155
118. Karolewski M, Cavell R, Gordon R, Glover C, Cheah M, Ridgway MC. 2013. Predicting XAFS scattering path cumulants and XAFS spectra for metals (Cu, Ni, Fe, Ti, Au) using molecular dynamics simulations. *J. Synchrotron Radiat.* 20:555–66
119. Timoshenko J, Anspoks A, Cintins A, Kuzmin A, Purans J, Frenkel AI. 2018. Neural network approach for characterizing structural transformations by X-ray absorption fine structure spectroscopy. *Phys. Rev. Lett.* 120:225502
120. Timoshenko J, Wrasman CJ, Luneau M, Shirman T, Cargnello M, et al. 2018. Probing atomic distributions in mono- and bimetallic nanoparticles by supervised machine learning. *Nano Lett.* 19:520–29
121. Kuzmin A, Evarestov R. 2009. Quantum mechanics–molecular dynamics approach to the interpretation of X-ray absorption spectra. *J. Phys. Condens. Matter* 21:055401
122. Anspoks A, Kalinko A, Kalendarev R, Kuzmin A. 2012. Atomic structure relaxation in nanocrystalline NiO studied by EXAFS spectroscopy: role of nickel vacancies. *Phys. Rev. B* 86:174114
123. Anspoks A, Kuzmin A. 2011. Interpretation of the Ni K-edge EXAFS in nanocrystalline nickel oxide using molecular dynamics simulations. *J. Non-Cryst. Solids* 357:2604–10
124. Anspoks A, Kalinko A, Kalendarev R, Kuzmin A. 2013. Probing vacancies in NiO nanoparticles by EXAFS and molecular dynamics simulations. *J. Phys. Conf. Ser.* 430:012027
125. Anspoks A, Kuzmin A, Kalinko A, Timoshenko J. 2010. Probing NiO nanocrystals by EXAFS spectroscopy. *Solid State Commun.* 150:2270–74
126. Oliver P, Watson G, Parker S. 1995. Molecular-dynamics simulations of nickel oxide surfaces. *Phys. Rev. B* 52:5323–29

127. Rousseau R, Schenter GK, Fulton JL, Linehan JC, Engelhard MH, Autrey T. 2009. Defining active catalyst structure and reaction pathways from ab initio molecular dynamics and operando XAFS: dehydrogenation of dimethylaminoborane by rhodium clusters. *J. Am. Chem. Soc.* 131:10516–24
128. Chen Z, Duan Z, Wang Z, Liu X, Gu L, et al. 2017. Amorphous cobalt oxide nanoparticles as active water oxidation catalysts. *ChemCatChem* 9:3641–45
129. Narayan O, Young AP. 2001. Convergence of Monte Carlo simulations to equilibrium. *Phys. Rev. E* 64:021104
130. Hansen PL, Molenbroek AM, Ruban AV. 1997. Alloy formation and surface segregation in zeolite-supported Pt–Pd bimetallic catalysts. *J. Phys. Chem. B* 101:1861–68
131. Molenbroek AM, Nørskov JK, Clausen BS. 2001. Structure and reactivity of Ni–Au nanoparticle catalysts. *J. Phys. Chem. B* 105:5450–58
132. Rehr J, Ankudinov A. 2005. Progress in the theory and interpretation of XANES. *Coord. Chem. Rev.* 249:131–40
133. Small MW, Sanchez SI, Marinkovic NS, Frenkel AI, Nuzzo RG. 2012. Influence of adsorbates on the electronic structure, bond strain, and thermal properties of an alumina-supported Pt catalyst. *ACS Nano* 6:5583–95
134. Behafarid F, Ono L, Mostafa S, Croy J, Shafai G, et al. 2012. Electronic properties and charge transfer phenomena in Pt nanoparticles on γ-Al_2O_3: size, shape, support, and adsorbate effects. *Phys. Chem. Chem. Phys.* 14:11766–79
135. Mazalova V, Soldatov A, Adam S, Yakovlev A, Möller T, Johnston R. 2009. Small copper clusters in Ar shells: a study of local structure. *J. Phys. Chem. C* 113:9086–91
136. Gorczyca A, Moizan V, Chizallet C, Proux O, Del Net W, et al. 2014. Monitoring morphology and hydrogen coverage of nanometric Pt/γ-Al_2O_3 particles by in situ HERFD–XANES and quantum simulations. *Angew. Chem.* 126:12634–37
137. Vila FD, Rehr JJ, Kelly SD, Bare SR. 2013. Operando effects on the structure and dynamics of Pt_nSn_m/γ-Al_2O_3 from ab initio molecular dynamics and X-ray absorption spectra. *J. Phys. Chem. C* 117:12446–57
138. Naicker PK, Cummings PT, Zhang H, Banfield JF. 2005. Characterization of titanium dioxide nanoparticles using molecular dynamics simulations. *J. Phys. Chem. B* 109:15243–49
139. Yamamoto T, Kobayashi H, Kumara LSR, Sakata O, Nitta K, et al. 2017. Disappearance of the superionic phase transition in sub-5 nm silver iodide nanoparticles. *Nano Lett.* 17:5273–76
140. Petkov V, Hessel CM, Ovtchinnikoff J, Guillaussier A, Korgel BA, et al. 2013. Structure–properties correlation in Si nanoparticles by total scattering and computer simulations. *Chem. Mater.* 25:2365–71
141. Gereben O, Petkov V. 2013. Reverse Monte Carlo study of spherical sample under non-periodic boundary conditions: the structure of Ru nanoparticles based on X-ray diffraction data. *J. Phys. Condens. Matter* 25:454211
142. Petkov V, Prasai B, Shastri S, Kim J-W, Shan S, et al. 2017. Surface atomic structure and functionality of metallic nanoparticles: a case study of Au–Pd nanoalloy catalysts. *J. Phys. Chem. C* 121:7854–66
143. Petkov V, Prasai B, Shastri S, Park H-U, Kwon Y-U, Skumryev V. 2017. Ensemble averaged structure–function relationship for nanocrystals: effective superparamagnetic Fe clusters with catalytically active Pt skin. *Nanoscale* 9:15505–14
144. Mejía-Rosales SJ, Fernández-Navarro C, Pérez-Tijerina E, Blom DA, Allard LF, José-Yacamán M. 2007. On the structure of Au/Pd bimetallic nanoparticles. *J. Phys. Chem. C* 111:1256–60
145. Krayzman V, Levin I. 2012. Reverse Monte Carlo refinements of nanoscale atomic correlations using powder and single-crystal diffraction data. *J. Appl. Crystallogr.* 45:106–12

Annual Review of
Analytical Chemistry

Volume 12, 2019

Contents

Wearable Sensors for Biochemical Sweat Analysis
Amay J. Bandodkar, William J. Jeang, Roozbeh Ghaffari, and John A. Rogers 1

E-Cigarette Chemistry and Analytical Detection
Robert M. Strongin 23

Emerging Analytical Techniques for Rapid Pathogen Identification and Susceptibility Testing
Dong Jin Shin, Nadya Andini, Kuangwen Hsieh, Samuel Yang, and Tza-Huei Wang 41

Polyvalent Nanoobjects for Precision Diagnostics
David T. Omstead, Jenna Sjoerdsma, and Basar Bilgicer 69

Whole-Organism Analysis by Vibrational Spectroscopy
Dale Christensen, Anja Rüther, Kamila Kochan, David Pérez-Guaita, and Bayden Wood 89

Recent Developments in Nanosensors for Imaging Applications in Biological Systems
Guoxin Rong, Erin E. Tuttle, Ashlyn Neal Reilly, and Heather A. Clark 109

Development and Applications of Bioluminescent and Chemiluminescent Reporters and Biosensors
Hsien-Wei Yeh and Hui-Wang Ai 129

Advances in Surface Plasmon Resonance Imaging and Microscopy and Their Biological Applications
Markéta Bocková, Jiří Slabý, Tomáš Špringer, and Jiří Homola 151

Challenges in Identifying the Dark Molecules of Life
María Eugenia Monge, James N. Dodds, Erin S. Baker, Arthur S. Edison, and Facundo M. Fernández 177

Metabolic Imaging at the Single-Cell Scale: Recent Advances in Mass Spectrometry Imaging
Ian S. Gilmore, Sven Heiles, and Cornelius L. Pieterse 201

Laser Desorption Combined with Laser Postionization for Mass Spectrometry
Luke Hanley, Raveendra Wickramasinghe, and Yeni P. Yung 225

Molecular Characterization of Atmospheric Organic Aerosol by Mass Spectrometry
Murray V. Johnston and Devan E. Kerecman 247

Electrochemiluminescence Imaging for Bioanalysis
Jingjing Zhang, Stéphane Arbault, Neso Sojic, and Dechen Jiang 275

Electrochemistry at the Synapse
Mimi Shin, Ying Wang, Jason R. Borgus, and B. Jill Venton 297

Advanced Spectroelectrochemical Techniques to Study Electrode Interfaces Within Lithium-Ion and Lithium-Oxygen Batteries
Alexander J. Cowan and Laurence J. Hardwick 323

Single Nanoparticle Electrochemistry
Fato Tano Patrice, Kaipei Qiu, Yi-Lun Ying, and Yi-Tao Long 347

Single-Molecule Analysis with Solid-State Nanopores
Tim Albrecht 371

Flow Cytometric Analysis of Nanoscale Biological Particles and Organelles
Hong Lian, Shengbin He, Chaoxiang Chen, and Xiaomei Yan 389

High-Parameter Single-Cell Analysis
Pratip K. Chattopadhyay, Aidan F. Winters, Woodrow E. Lomas III, Andressa S. Laino, and David M. Woods 411

Single-Cell Protein Secretion Detection and Profiling
Zhuo Chen, Jonathan J. Chen, and Rong Fan 431

Well-Defined Materials for High-Performance Chromatographic Separation
Yu Liang, Lihua Zhang, and Yukui Zhang 451

Separation Phenomena in Tailored Micro- and Nanofluidic Environments
Mukul Sonker, Daihyun Kim, Ana Egatz-Gomez, and Alexandra Ros 475

Solving the Structure and Dynamics of Metal Nanoparticles by Combining X-Ray Absorption Fine Structure Spectroscopy and Atomistic Structure Simulations
J. Timoshenko, Z. Duan, G. Henkelman, R.M. Crooks, and A.I. Frenkel 501

Imaging and Analytics on the Helium Ion Microscope
Tom Wirtz, Olivier De Castro, Jean-Nicolas Audinot, and Patrick Philipp 523

Errata

An online log of corrections to *Annual Review of Analytical Chemistry* articles may be found at http://www.annualreviews.org/errata/anchem